AAS 14-393

A GAS BEARING PLATFORM ATTITUDE CONTROL FOR ASSESSMENT OF AOCS SYSTEMS

V. Carrara[*], A. M. Oliveira[†] and H. K. Kuga[‡]

This paper presents a solution for the development, validation and testing of attitude control system for satellites with hardware-in-the-loop dynamics and control. The system is based on a gas-bearing platform in which several sensors and actuators, similar to those usually employed in satellites (engineering models) were fixed. Magnetometers and gyroscopes are easily incorporated to the platform, but sun sensors and star sensors are more difficult. The solar sensors are replaced by a tri-axes accelerometer, while the star sensor relies on direct night sky measurements. Although hot gas thrusters cannot be used, both magnetic torque coils and reaction wheels are feasible to be incorporated to the arrangement. The gas-bearing balancing process is critical for real satellite dynamic simulation and therefore the solution is addressed in this work, by means of a non-linear filtering of the sensor readings. The filtering process also obtains the platform mass properties. In order to increase the filter accuracy the gyroscopes were calibrated; the calibration results are also presented here. Finally, an attitude controller was implemented in the platform and the control performance was analyzed and shown together with the conclusions.

INTRODUCTION

During recent years the development of Attitude and Orbit Control Systems (AOCS) for small satellites has been spread from large industries and space agencies to universities and small companies. This change was mainly caused by cost reduction due to miniaturization and large-scale production of electronic components. Software design and qualification tests nevertheless still remain an expensive part of AOCS development costs. However, AOCS qualification tests are taking advantage of the benefits of Gas-Bearing Platforms (GBP), which have now affordable prices.

GBP have been widely used over the past 50 years to simulate the free-of-torque frictionless space conditions and environment. In the United States, the earliest record of a 3-Degrees-Of-Freedom (DOF) bearing for attitude simulation of a satellite was in 1959 at U.S. Army Ballistic Missile Agency[1]. That GBP was later incorporated to the NASA's Marshall Space Flight Center. In mid-1990, the use of this technology for simulating a free of torque environment was already quite common at many universities scattered across North America, Europe and Japan. The basic

[*] Doctor, Space Mechanics and Control Division, National Institute for Space Research - INPE, SJCampos-SP, Brazil.
[†] MSc, Space Mechanics and Control Division, National Institute for Space Research - INPE, SJCampos-SP, Brazil.
[‡] Doctor, Space Mechanics and Control Division, National Institute for Space Research - INPE, SJCampos-SP, Brazil.

experiments conducted by universities are linked to the areas of attitude control[2,3], parameter estimation[4,5,6] and validation of space subsystems, including actuators and sensors in general.

Today the main purpose of such platforms is to study methods of three-axis satellite attitude stabilization and control. Several industries, agencies and universities are investing in this technology envisaging design enhancement, reliability improvement, cost reduction and shortening of the development time. On the other hand the balancing process of the platform is still a major problem, since any unbalancing mass can easily cause a torque larger than the ones found in space environment. So, balancing should assure that the platform center of mass remains close to the bearing center by amounts estimated in less than few tenths of microns.

To achieve the goal of developing a three-axis AOCS to meet the upcoming Brazilian missions, a dumbbell type GBP (300 pounds capacity) was equipped with several sensors (gyroscopes, star sensor, magnetometer and GPS receiver) and actuators (3 reaction wheels and 3 magnetic torque coils), with characteristics similar to the equipment that will be employed in those missions. All equipment have been integrated to a PCDH (Power Conditioning and Data Handling) computer capable of managing the power and data transmitted to and coming from each one. Additionally the GBP was placed in a room with retractile ceiling in order to allow star sensor readings at night.

The validation of the simulation environment, the synthesis of the control system, and the controller performance depend on the accurate knowledge of mass distribution of the platform, more precisely the moments of inertia and center of mass. A non-linear filter based on data gathered from the sensors estimates those properties with the desired accuracy, and will be presented in this work. Finally, a control algorithm has been proposed to stabilize the platform in the three axes using the reaction wheels with orthogonal arrangement. The attitude determination procedure is based on measurements of three gyroscopes, also oriented orthogonal to each other and a star sensor. The characteristic curves of the sensors and actuators used in the simulation were based on the ICD (Interface Control Document) of the equipment and characterization experiments. Several experiments can be done in the GBP, such as AOCS operation modes validation and testing, sensors and actuators identification and characterization, and control algorithm validation in a realistic hardware-in-the-loop network. This paper presents the balancing process, the gyros characterization procedures and results, the mass properties estimation process and some results coming from a basic GBP attitude control.

THE GAS-BEARING PLATFORM

The platform consists of a dumbbell shape spherical gas bearing, shown in Figure (1). It has 360^{o} revolution in two axes and the motion is limited to 30^{o} around the symmetric axis. The platform is equipped with 3 reaction wheels, 3 magnetic torque coils, a star tracker, a gyroscope triad, a 3-axis magnetometer, a GPS receiver, a programmable Power Condition and Data Handling unit (PCDH) for attitude control logic, a 28 V Li-Ion battery and a wireless communication data link through RS232 serial interface. The platform is now operating at the Simulation Laboratory (LABSIM) of INPE (National Institute for Space Research) in Brazil. All the sensors, actuators, battery and control computer are engineering models.

The maximum momentum storage for the reaction wheel is 2.65 Nms at 6100 rpm, with maximum torque of 0.025 Nm. The reaction wheel operates in both torque control and speed control operating modes, including torque compensation for high motor temperature.

The star tracker has a field of view of 14^{o} squared, with sampling rate of 4 Hz when in tracking mode. Lost in space acquisition takes less than 5 seconds. The accuracy is 18 arc-sec in

the sensor plane and 122 arc-sec around the sensor axis. The predecessors of this sensor were successfully employed on TUBSAT-A and MAROC-TUBSAT micro-satellites from Technical University of Berlin. It provides reliable readings in clear night skies, even in presence of moonlight or city lights. Although atmospheric refraction is not compensated for in measurements, it is considered that the sensor readings are still accurate, since the sensor will operate normally close to the zenithal direction.

The magnetic torques can generate up to ±10 Am^2 of magnetic dipole in its axis direction. The magnetometer uses magnetic resistive element sensors to achieve 4 mGauss accuracy at 6 kHz maximum sampling rate.

The gyroscope triad is composed of three Northrop Grumman μFORS-6U fiber optic rate sensors. The characterization and calibration procedures were performed in a precise servo-controlled turntable, and will be described in the next section.

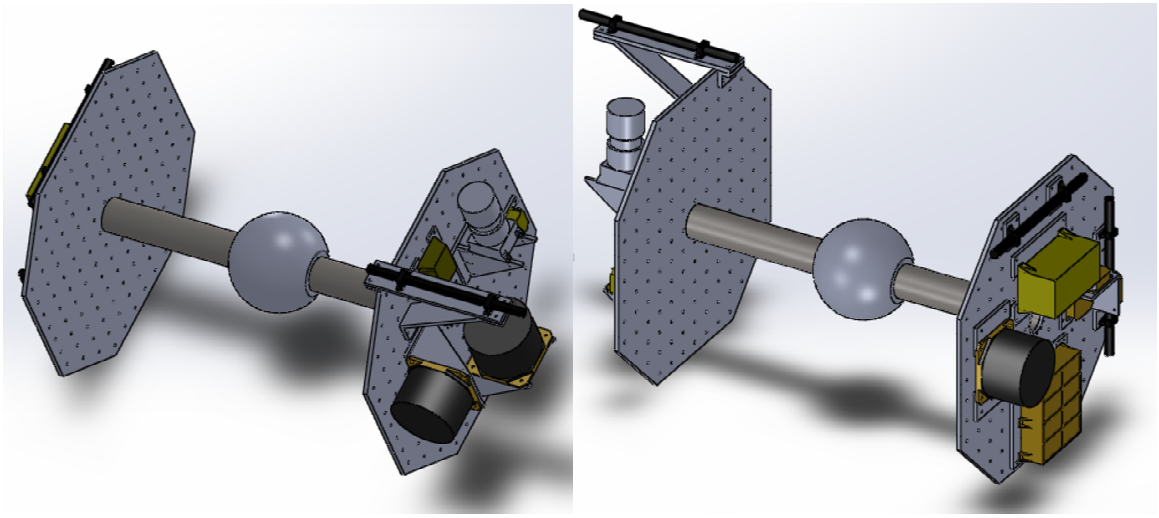

Figure 1. The spherical gas bearing platform.

Gyroscope triad characterization

It is desirable to find the following characterization coefficients for the gyroscope triad:

$$\tilde{\boldsymbol{\omega}} = \mathbf{S}\,\boldsymbol{\omega} + \mathbf{b} \tag{1}$$

where $\boldsymbol{\omega}$ is the vector with the reference values for the angular velocity, $\tilde{\boldsymbol{\omega}}$ is the vector of measurements obtained by the sensor triad, $\mathbf{b}$ is the vector of offsets and $\mathbf{S}$ takes into account both the misalignment between the gyros and the output axis, and the gyro scale factors.

Based on the linear model, the measure vector is:

$$\mathbf{y} = \mathbf{H}\,\mathbf{x} \tag{2}$$

where $\mathbf{y}$ is the gyro measurements. A set of 6 data sets were generated in which each triad axis was oriented in the vertical direction both up and down. For each data set, the turntable was commanded to turn 360° around the vertical direction with a given angular velocity plus 10 seconds. The reference angular rates were ±0.75°/s, ±0.5°/s ±0.25°/s and null angular velocity

(with 1450 seconds duration), as can be seen in the example of Figure (2) for the first sequence in the gyro *x*-axis. All other data sets follow similar profiles. For each reference angular rate a unique mean value of the measured data was then calculated and stored in **y** vector in the sequence:

$$\mathbf{y} = \tilde{\boldsymbol{\omega}} = \left[\tilde{\omega}_x(1) \quad \cdots \quad \tilde{\omega}_x(6) \quad \tilde{\omega}_y(1) \quad \cdots \quad \tilde{\omega}_y(6) \quad \tilde{\omega}_z(1) \quad \cdots \quad \tilde{\omega}_z(6) \right]^T \tag{3}$$

where $\tilde{\omega}_i(j)$, with $i = x, y, z$ is the vector of measurements for each one of the 6 sequences.

Hence, there are six data sequences for each axis. The vector of parameters to be estimated is:

$$\mathbf{x} = \left[S_{xx} \quad S_{xy} \quad S_{xz} \quad b_x \quad S_{yx} \quad S_{yy} \quad S_{yz} \quad b_y \quad S_{zx} \quad S_{zy} \quad S_{zz} \quad b_z \right]^T \tag{4}$$

where S_{ij} and b_i are the components of matrix **S** and bias vector **b**, respectively.

The **H** matrix is therefore defined as:

$$\mathbf{H} = \begin{bmatrix} \mathbf{H}(\omega_{ref}) & \mathbf{0} & \mathbf{0} \\ \mathbf{0} & \mathbf{H}(\omega_{ref}) & \mathbf{0} \\ \mathbf{0} & \mathbf{0} & \mathbf{H}(\omega_{ref}) \end{bmatrix} \tag{5}$$

where **H**(ω) is the sub-matrix

$$\mathbf{H}(\omega_{ref}) = \begin{bmatrix} \omega_{ref} & 0 & 0 & 1 \\ -\omega_{ref} & 0 & 0 & 1 \\ 0 & \omega_{ref} & 0 & 1 \\ 0 & -\omega_{ref} & 0 & 1 \\ 0 & 0 & \omega_{ref} & 1 \\ 0 & 0 & -\omega_{ref} & 1 \end{bmatrix} \tag{6}$$

and ω_{ref} is the reference angular velocity imposed by the precision turntable.

By reducing the cost-index **L** based on the square of residues:

$$\mathbf{L} = \left(\mathbf{y} - \mathbf{H}\,\mathbf{x}\right)^T \mathbf{W} \left(\mathbf{y} - \mathbf{H}\,\mathbf{x}\right) \tag{7}$$

the best vector **x** is estimated, which minimizes the cost-index and therefore are the best values for the linear model of the calibrated gyroscope triad. The weight-matrix **W** is the gyro's covariance matrix, defined by:

$$\mathbf{W} = \begin{bmatrix} 1/\sigma_x^2(1) & \cdots & \mathbf{0} \\ \vdots & \ddots & \vdots \\ \mathbf{0} & \cdots & 1/\sigma_z^2(6) \end{bmatrix} \tag{8}$$

where $\sigma_i(j)$ is the data standard deviation over *i* axis and sequence *j*. The vector $\hat{\mathbf{x}}$ can be obtained by[7]:

$$\hat{\mathbf{x}} = \mathbf{P}\,\mathbf{H}^T\,\mathbf{W}\,\mathbf{y} \tag{9}$$

where the state covariance matrix **P** can be found by solving:

$$\mathbf{P} = \left(\mathbf{H}^T\,\mathbf{W}\,\mathbf{H}\right)^{-1} \tag{10}$$

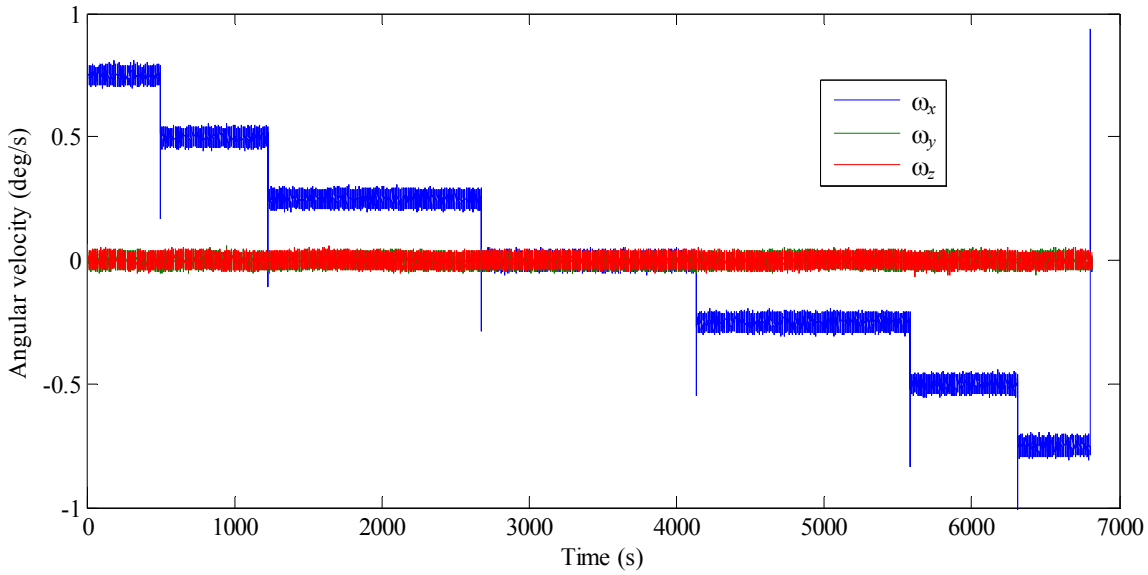

Figure 2. Gyroscope triad measurement from sequence 1 (x axis is vertical).

Crude acquired data needs to be processed before running into the algorithm. As can be seen in Figure (3) with the angular velocity of the turntable adjusted to 0.5º/s and the gyro *x*-axis in the up direction, the Earth's rotation rate can be detected by the gyros. In fact, both *y* and *z* axes show a slight oscillation caused by the Earth's rate, which needs to be subtracted from the collected data by:

$$\boldsymbol{\omega}_{cor} = \boldsymbol{\omega}_{msr} - \Omega_E \left[\sin\psi \quad \cos\psi\cos(\omega_{ref}t + \theta_0) \quad \cos\psi\sin(\omega_{ref}t + \theta_0)\right]^T \tag{11}$$

where ψ is the local latitude of the experiment, θ_0 is the initial angular position of the turntable and Ω_E is the Earth's angular velocity. $\boldsymbol{\omega}_{cor}$ and $\boldsymbol{\omega}_{msr}$ stand respectively for the corrected and crude measurements. A simple mean value of $\boldsymbol{\omega}_{cor}$ on *m* measurements, for each of the reference angular velocities of the turntable composes the $\tilde{\boldsymbol{\omega}}(j)$ vector, with j = 1, …, 6. Obviously, also for each one of the sequences, the element position changes in the vector. The axis in vertical direction is always subtracted by the sin(ψ) component. Finally, after getting 7 calibration parameter sets, one for each reference angular velocity they are composed in a single one by weighing with its covariance term.

The misalignment matrix **S** and the bias vector **b** after least squares processing were

$$\mathbf{S} = \begin{bmatrix} 0.999998 & 0.001119 & -0.001261 \\ -0.000909 & 0.999999 & 0.000079 \\ 0.002063 & 0.001298 & 0.999996 \end{bmatrix} \tag{12}$$

$$\mathbf{b} = \begin{bmatrix} 0.0003152 & -0.0007884 & 0.0001749 \end{bmatrix}^T \text{°/s} \tag{13}$$

and it is easy to see that the maximum estimated misalignment was around 0.1 degrees. The standard deviation matrix of the misalignment **S** and the standard deviation vector for the bias resulted, respectively:

$$\boldsymbol{\sigma}_{\mathbf{S}} = \begin{bmatrix} 0.021817 & 0.022299 & 0.022371 \\ 0.019699 & 0.019518 & 0.019678 \\ 0.020059 & 0.020120 & 0.020037 \end{bmatrix} \tag{14}$$

$$\boldsymbol{\sigma}_{\mathbf{b}} = \begin{bmatrix} 0.0052344 & 0.0046380 & 0.0047413 \end{bmatrix}^T \text{°/s} \tag{15}$$

For data validation the slowest rate of 0.25°/s was chosen in order to perform the determination of the angular position after a full turn of 360 degrees, during 1440 seconds, around the *x*-axis. Earth's angular velocity was removed from the data prior this analysis. Without the correction in the angular measurements of Equation (1), the integrated angular rate resulted $\Delta\theta = \begin{bmatrix} 360.4499 & -1.7441 & 0.8332 \end{bmatrix}^T$ degrees, while the error was clearly smaller when the correction was done, resulting from the integrated rate of $\Delta\theta = \begin{bmatrix} 360.1197 & -0.9061 & 0.5281 \end{bmatrix}^T$ degrees.

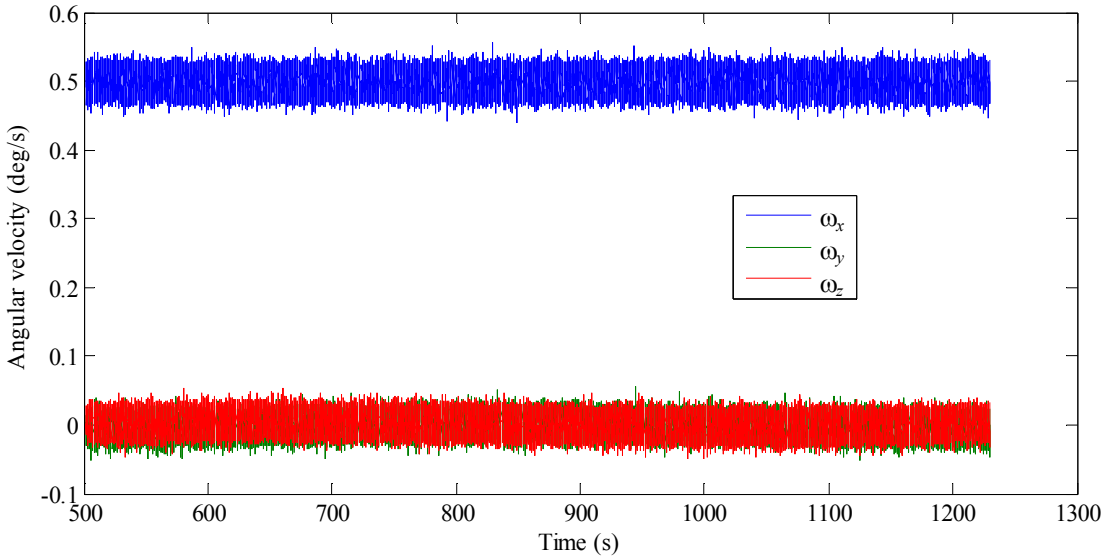

Figure 3. Small sinusoidal pattern (ω_y and ω_z) of the gyroscope triad measurement due Earth's angular velocity.

THEORETICAL BASIS

This section starts with a brief description of the attitude kinematics and dynamics of a rigid body, and is supplemented with a description of the estimation algorithm and the characterization experiment for the gyroscope triad.

Attitude kinematics and dynamics

Attitude kinematics of a generic body can be described in different modes. Usually, Euler angles or quaternions are used. The use of quaternions is justified by computational facility, since trigonometric functions are avoided, circumventing computational problems like divisions by zero. On the other hand, it presents some difficulty for attitude estimation due to the lack of independence of the four quaternions, which are related by the constraint that the quaternion has unit magnitude. This constraint results in a singularity of the quaternion covariance matrix[8]. Within this perspective, the Euler angles are usually adopted for attitude propagation in the filtering prediction phase. The body attitude with respect to the inertial reference frame can be represented by three rotations that align these two distinct reference systems. In the LVLH (Local Vertical, Local Horizontal) system (x towards East, y towards North, z to zenith), the motion around the x-axis is assumed as pitch (θ), around the y-axis is roll (φ) and around the z-axis is heading (ψ). For the time interval of the experiments seen here the Earth's rotation rate can be neglected and so the LVLH coordinate system can be considered as a inertial system. Hence, the rotation sequence used in this work for Euler angles is 3-2-1 represented by the following transformation of matrix[9,10]:

$$\mathbf{C}_{br} = \begin{bmatrix} \cos\varphi\cos\psi & \cos\varphi\sin\psi & -\sin\varphi \\ \sin\varphi\sin\theta\cos\psi - \cos\varphi\sin\psi & \sin\varphi\sin\theta\sin\psi + \cos\varphi\cos\psi & \sin\varphi\cos\theta \\ \cos\varphi\sin\theta\cos\psi + \sin\varphi\sin\psi & \cos\varphi\sin\theta\sin\psi - \sin\varphi\cos\psi & \cos\varphi\cos\theta \end{bmatrix} \tag{16}$$

The set of kinematics equations are therefore given by:

$$\begin{bmatrix} \dot{\varphi} \\ \dot{\theta} \\ \dot{\psi} \end{bmatrix} = \begin{bmatrix} 1 & \sin\varphi\tan\theta & \cos\varphi\tan\theta \\ 0 & \cos\varphi & -\sin\varphi \\ 0 & \sin\varphi/\cos\theta & \cos\varphi/\cos\theta \end{bmatrix} \begin{bmatrix} \omega_x \\ \omega_y \\ \omega_z \end{bmatrix} \tag{17}$$

where ω_x, ω_y and ω_z are the angular velocity measured at the body reference system. The angular momentum law with respect to an inertial frame defines the attitude dynamics of a rigid body:

$$\dot{\mathbf{h}} = \mathbf{T} \tag{18}$$

where $\mathbf{h}$ is the angular momentum vector defined as:

$$\mathbf{h} = \mathbf{I}\,\boldsymbol{\omega} \tag{19}$$

in which $\mathbf{I}$ is the body inertia matrix and $\boldsymbol{\omega}$ is the angular velocity vector. $\mathbf{T}$ is the sum of external torques, divided into environmental and control torques, defined by:

$$\mathbf{T} = \mathbf{T}_{env} + \mathbf{T}_{con} \tag{20}$$

When expressed in a frame attached to the body, the attitude dynamics of a rigid body is represented by:

$$\mathbf{I}\,\dot{\boldsymbol{\omega}} + \boldsymbol{\omega} \times \mathbf{I}\,\boldsymbol{\omega} = \mathbf{T} \tag{21}$$

Thus, the rigid body dynamics is a nonlinear function of the angular velocity vector and the external torque:

$$\dot{\boldsymbol{\omega}} = \mathbf{I}^{-1}\,(\mathbf{T} - \boldsymbol{\omega} \times \mathbf{I}\,\boldsymbol{\omega}) \tag{22}$$

The environmental torque $\mathbf{T}_{CG}$ caused by the displacement of the center of gravity of the platform with respect to the bearing center is obtained by:

$$\mathbf{T}_{CG} = \mathbf{R}_{CG} \times \mathbf{P} \tag{23}$$

where $\mathbf{R}_{CG}$ is the center of gravity position vector of the bearing with respect to the bearing rotation center and $\mathbf{P}$ is the weight vector. It can be noted that the vector $\mathbf{R}_{CG}$ is measured in body system reference while the vector $\mathbf{P}$ is known in topocentric reference system:

$$\mathbf{P} = \begin{bmatrix} 0 & 0 & -m\,g \end{bmatrix}^T \tag{24}$$

where m is the total mass of the platform and g is the local gravity acceleration. Since the torque shall be expressed in the body reference system, Equation (23) must be changed to:

$$\mathbf{T}_{CG} = \mathbf{R}_{CG} \times (\mathbf{C}_{br}\ \mathbf{P}) \tag{25}$$

where $\mathbf{C}_{br}$ is the rotation matrix defined in Equation (16).

Extended Kalman filtering

Kalman filter, in its standard form, is an optimal minimum variance estimator that incorporates uncertainties both in the dynamic and observation models. However, Kalman filter can handle only linear systems, while its non-linear version, the Extended Kalman Filter (EKF), applies to any continuous dynamics. Unlike its linear version, the EKF is not optimal due to truncation of higher order terms.

Extended Kalman Filter is a state estimation algorithm that, with some adjustments, can also be used for parameter estimation. It is the generalization of the Kalman filter for nonlinear dynamic systems. Most references on the subject divides the algorithm into two phases: prediction and correction[11,12]. Here a generic system with input vector $\mathbf{u}$, state vector $\mathbf{x}$ and measurement vector $\mathbf{y}$, is described by:

$$\dot{\mathbf{x}} = \mathbf{f}(\mathbf{x}, \mathbf{u}, t) + \mathbf{w}_k \tag{26}$$

$$\mathbf{y}_{k+1} = \mathbf{h}_{k+1}(\mathbf{x}_{k+1}) + \mathbf{v}_{k+1} \tag{27}$$

where $\mathbf{f}$ and $\mathbf{h}_k$ are nonlinear functions linking the state vector $\mathbf{x}$ to the dynamic and the observation models, respectively. The process and observation noises are represented by random variables $\mathbf{w} = \mathbf{N}(0, \mathbf{Q})$ and $\mathbf{v}_k = \mathbf{N}(0, \mathbf{R})$, Gaussian distributions with zero mean and covariance $\mathbf{Q}$ and $\mathbf{R}$, in this sequence. It can be noted that the system prediction is continuous and the observation is discrete. For $\mathbf{x} \in \mathbf{R}$, the covariance matrix $\mathbf{P}$ has dimension $n \times n$ and is defined as:

$$\mathbf{P} = \mathrm{cov}[\mathbf{x}] = E[(\mathbf{x} - E[\mathbf{x}])(\mathbf{x} - E[\mathbf{x}])^T] = E[\mathbf{x}\mathbf{x}^T] - E[\mathbf{x}]E[\mathbf{x}]^T \tag{28}$$

where the function $E[\mathbf{x}]$ is the mathematical expectation.

The first phase of the EKF is based entirely on the system dynamics. Given the initial state vector $\mathbf{x}_0$ at time t_0, and knowing the input $\mathbf{u}$ applied over time, the system states can be propagated and therefore predicted in any time t_i, with $t_i > t_0$. This propagation is therefore done via numerical integration of the Equation (22) considering no uncertainty.

For the covariance prediction, the continuous Ricatti equation, that incorporates the uncertainty of each state equation of the model to the covariance matrix, is used:

$$\dot{\mathbf{P}} = \mathbf{F}\,\mathbf{P} + \mathbf{P}\,\mathbf{F}^T + \mathbf{G}\,\mathbf{Q}\,\mathbf{G}^T \tag{29}$$

where $\mathbf{G}$ is the association matrix between the process noise and the covariance. $\mathbf{F}$ is the Jacobian of $\mathbf{f}$, defined by:

$$\mathbf{F} = D\mathbf{f}(\mathbf{x}) = \begin{bmatrix} \frac{\partial f_1}{\partial x_1} & \cdots & \frac{\partial f_1}{\partial x_n} \\ \vdots & \ddots & \vdots \\ \frac{\partial f_n}{\partial x_1} & \cdots & \frac{\partial f_n}{\partial x_n} \end{bmatrix} \tag{30}$$

The correction process is done by comparing the obtained measurement from the predicted state $\mathbf{x}_{k+1}$ with the actual value of $\mathbf{y}_{k+1}$ obtained by the sensor at time t_1, with $t_1 > t_0$. The balance (weighing) between the predicted values and the values obtained by the sensors is given by the Kalman gain $\mathbf{K}_{k+1}$. Thus, the equations that summarize the correction process are:

$$\mathbf{K}_{k+1} = \overline{\mathbf{P}}_{k+1}\,\mathbf{H}_{k+1}^T \left(\mathbf{H}_{k+1}\,\overline{\mathbf{P}}_{k+1}\,\mathbf{H}_{k+1}^T + \mathbf{R}_{k+1}\right)^{-1} \tag{31}$$

$$\hat{\mathbf{P}}_{k+1} = \left(\mathbf{I} - \mathbf{K}_k\,\mathbf{H}_{k+1}\right)\overline{\mathbf{P}}_{k+1} \tag{32}$$

$$\boldsymbol{\Delta}_{k+1} = \mathbf{y}_{k+1} - \mathbf{h}(\overline{\mathbf{x}}_{k+1}) \tag{33}$$

$$\hat{\mathbf{x}}_{k+1} = \overline{\mathbf{x}}_{k+1} + \mathbf{K}_{k+1}\,\boldsymbol{\Delta}_{k+1} \tag{34}$$

where $\overline{\mathbf{P}}$ is the predicted covariance matrix and $\hat{\mathbf{P}}$ is the corrected covariance matrix.

The vector $\mathbf{x}_{k+1}$ is the best estimate for the state at the discrete time $k + 1$. The residue $\boldsymbol{\Delta}_{k+1}$ is defined as the difference between the sensor measurement and the value of the nonlinear function $\mathbf{h}$ applied to $\mathbf{x}_{k+1}$. The matrix $\mathbf{H}$ is the Jacobian of $\mathbf{h}$, applied at the point $\mathbf{x}_{k+1}$, and defined by:

$$\mathbf{H} = D\mathbf{h}(\mathbf{x}) = \begin{bmatrix} \frac{\partial h_1}{\partial x_1} & \cdots & \frac{\partial h_1}{\partial x_n} \\ \vdots & \ddots & \vdots \\ \frac{\partial h_n}{\partial x_1} & \cdots & \frac{\partial h_n}{\partial x_n} \end{bmatrix}_{k+1} \tag{35}$$

With the already computed $\hat{\mathbf{x}}_{k+1}$ and $\hat{\mathbf{P}}_{k+1}$ the algorithm is fed back, restarting the prediction and correction.

MASS PROPERTIES ESTIMATION

The mass properties, like satellite inertia and center of mass position, are measured on ground by special machines, named MOI measurement instruments. These machines require that the body have a rigid flange in order to be attached to the measurement instrument. However, GBP normally doesnot have a flange interface. Moreover, the instrument accuracy of CG position is far from desirable, for about 3 orders of magnitude. In fact it is easy to demonstrate that a misalignment of the CG from the bearing center larger than few micrometers can generate an attitude disturbance torque greater than those present in space. There are several methods and algorithms to measure and to estimate the mass properties of an unconstrained body[13]. In this section a procedure based on parameter estimation by an extended Kalman filter will be presented. This procedure was used to estimate the mass properties of the GBP of LABSIM shown previously, and the results will be detailed here.

The GBP was firstly manually balanced, so the remaining unbalance was minimized. The GBP was then released in a free motion, with a random angular velocity less than 0.5^{o}/s, and data was acquired at 2 Hz sampling frequency during 250 seconds. The measured data is composed by the gyros measurements only. Angular position was obtained by direct integration of the kinematics equations in Euler angles, as described by Equation (17), with adopted null angles at initial time. However, prior starting to estimate mass parameters the GBP was left to drift freely during few seconds.

The state to be estimated by the EKF was the integrated angular velocity, the GBP angular rate, the inertia moments and products, and the CG position:

$$\mathbf{x} = \begin{bmatrix} \varphi & \theta & \psi & \omega_x & \omega_y & \omega_z & I_{xx} & I_{yy} & I_{zz} & I_{xy} & I_{xz} & I_{yz} & R_{CGx} & R_{CGy} & R_{CGz} \end{bmatrix}^T \tag{36}$$

The measurement vector **y** is of course given by the integrated gyro measurements from the kinematics equations and the gyro measurements themselves:

$$\mathbf{y} = \begin{bmatrix} \varphi & \theta & \psi & \omega_x & \omega_y & \omega_z \end{bmatrix}^T \tag{37}$$

Since the observation vector is composed by the state vector Euler angles and angular velocity, the **H** matrix is formed by a 6^{th} order identity followed by a 6×9 null matrix. The dynamic Jacobian **F**, however, is far from simple. It was computed by the symbolic algebraic manipulator of Matlab, and the expressions resulted too long to be presented here.

The initial conditions for the EKF estimator of the state vector, state covariance matrix **P**, process covariance matrix **Q** and observation covariance matrix **R** were

$$
\begin{aligned}
\begin{bmatrix}\varphi & \theta & \psi\end{bmatrix}^T &= \begin{bmatrix}0.5955 & -0.0650 & -7.4421\end{bmatrix}^T \text{ rad} \\
\begin{bmatrix}\omega_x & \omega_y & \omega_z\end{bmatrix}^T &= \begin{bmatrix}0.0099 & -0.1655 & -0.2260\end{bmatrix}^T \text{ rad/s} \\
\mathbf{I} &= \begin{bmatrix}3 & 0 & 0 \\ 0 & 12 & 0 \\ 0 & 0 & 12\end{bmatrix} \text{ kg m}^2 \\
\mathbf{R}_{CG} &= \begin{bmatrix}0 & 0 & 0\end{bmatrix}^T \text{ m} \\
\mathbf{P} &= \text{diag}\begin{pmatrix}1 & 1 & 1 & 1 & 1 & 1 & 1 & 4 & 1 & 1 & 1 & 0.0001 & 0.0001 & 0.0001 & 0.0001\end{pmatrix} \\
\mathbf{R} &= \text{diag}\begin{pmatrix}7.615\,10^{-7} & 7.615\,10^{-7} & 7.615\,10^{-7} & 3.685\,10^{-6} & 3.685\,10^{-6} & 3.685\,10^{-6}\end{pmatrix} \\
\mathbf{Q} &= \text{diag}\begin{pmatrix}0 & 0 & 0 & 10^{-9} & 10^{-9} & 10^{-9} & 0 & 0 & 0 & 0 & 0 & 0 & 10^{-14} & 10^{-14} & 10^{-14}\end{pmatrix}
\end{aligned}
\tag{38}
$$

The initial moments of inertia were obtained via CAD model. It can be noted that the uncertainty to the model was only added to the dynamic model, Equation (22). Kinematics model was considered perfect in this method. Initial values for **P**, **Q** and **R** were based on gyro noise statistics and trial adjustment for filter convergence, or refining process, also called filter tuning. Figures (4) and (5) shows the data collected from angular position and angular velocity of the GBP. It can be seen that the platform completed 11 full turns around the *z*-axis (ψ) in 250 seconds.

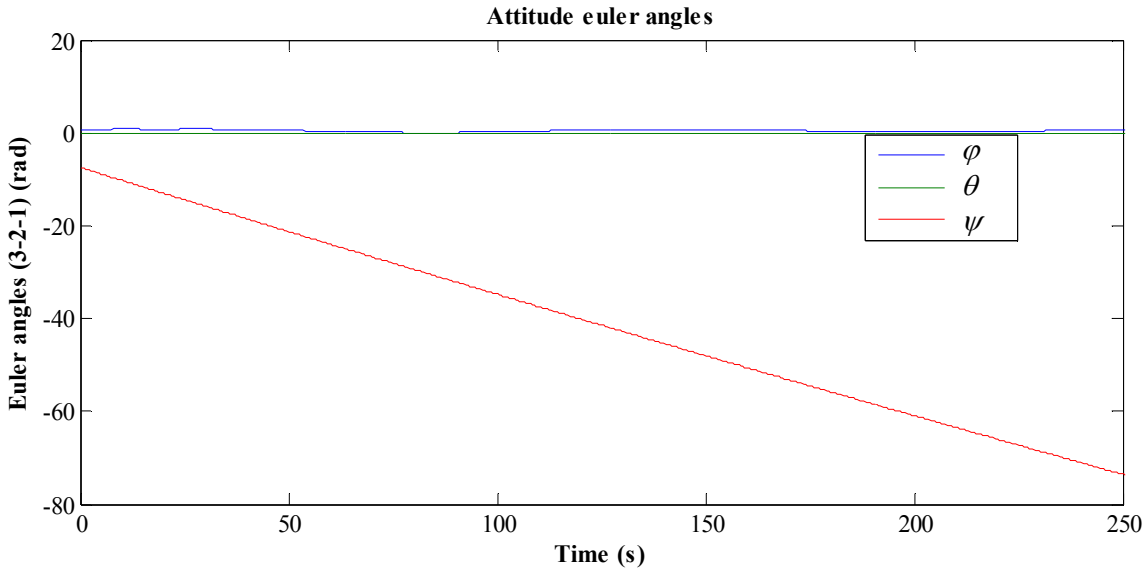

Figure 4. Euler angles of the GBP with sample time of 2 Hz.

Figures (6) and (7) show the estimated mass properties of the GBP as function of the time. The median curve is the mean value of each parameter. Above and below curves show the parameter added and subtracted with one standard deviation at the corresponding time. Although the mass properties given by the CAD program showed reasonable agreement with the final values, the filter obtained not only the inertia moments but also non-null inertia products (I_{xx}, I_{xy} and I_{xz}). It's remarkable that the CG position, whose filter estimate is presented in Figure (7), resulted less than 10 micrometers after the manual balancing.

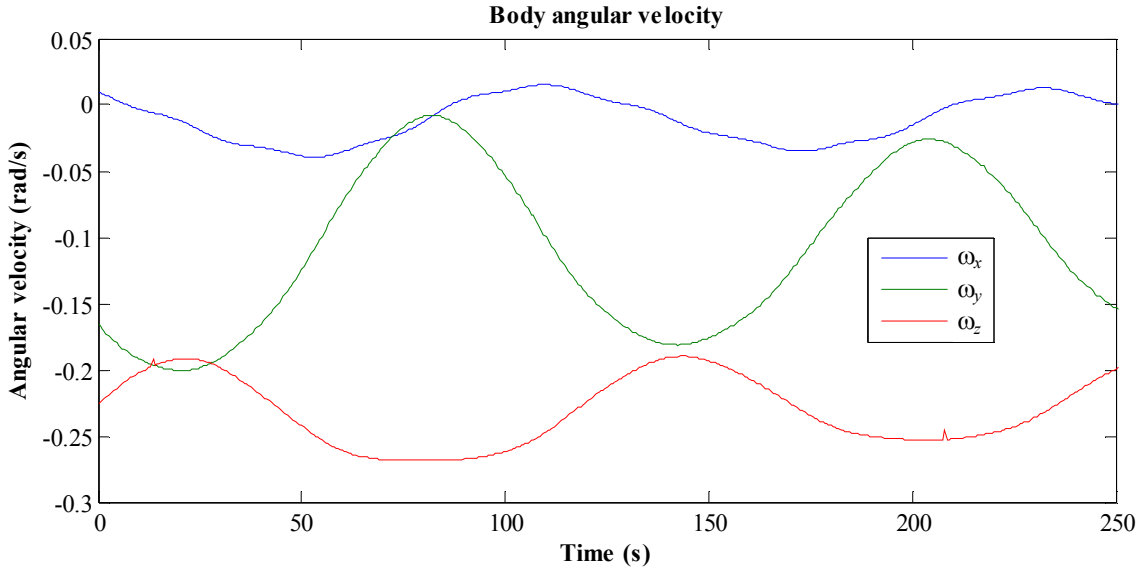

Figure 5. Data collected for angular velocity with sample time of 2 Hz.

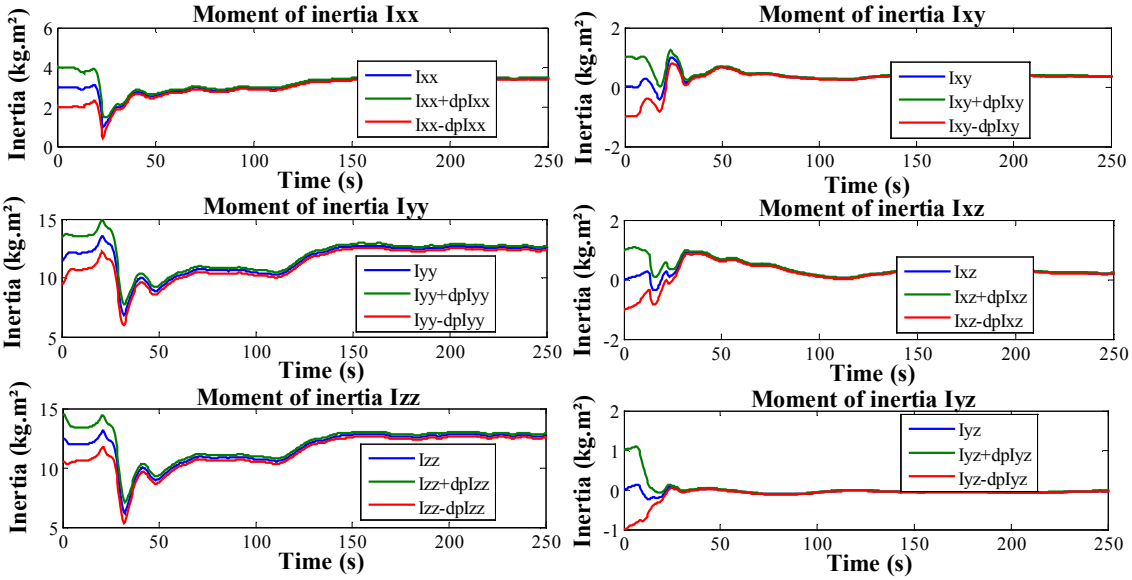

Figure 6. Estimated moments of inertia.

The residues from the measurements of angular position and angular velocity during the estimation process are shown on Figures (8), Euler angles, and (9), angular velocities. It is well established that estimation algorithm is working properly when the residues are close to zero. The angular position error is less than 0.6^{o} after filter convergence, while the angular rate remained below 0.23^{o}/s.

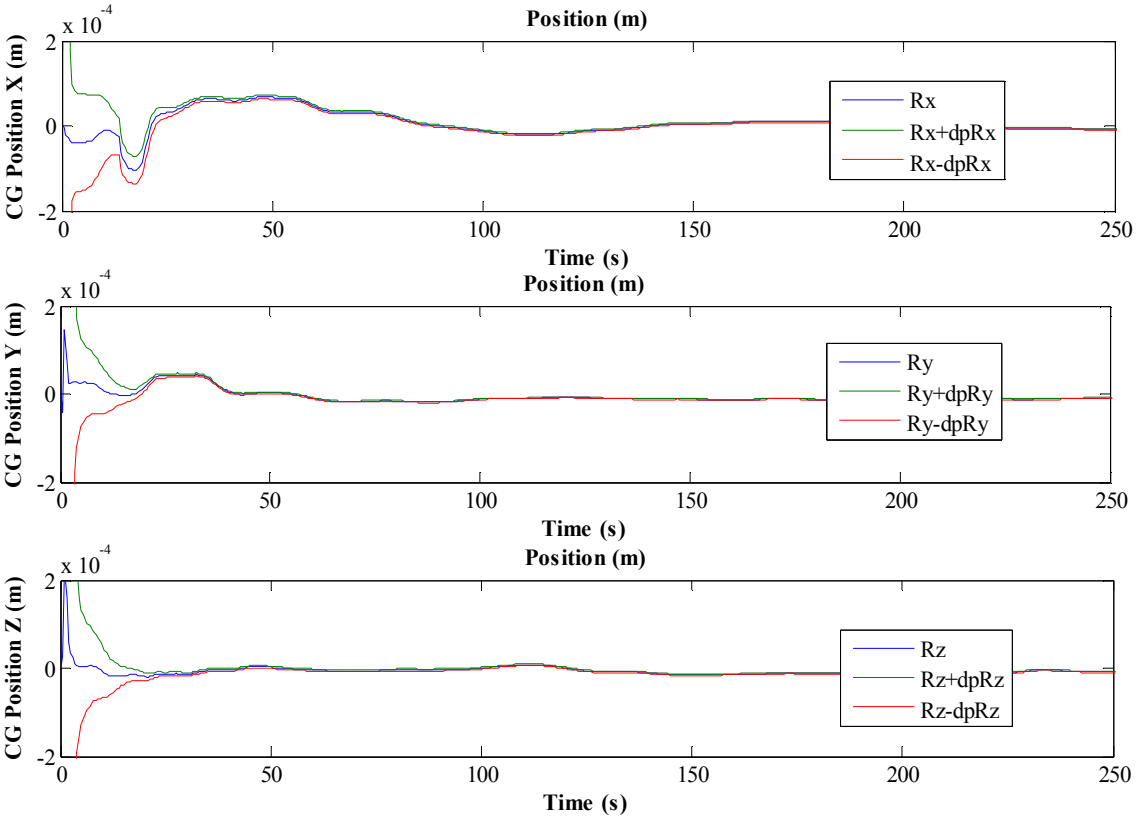

Figure 7. Estimated position of the center of gravity in three dimensions.

The final values for the GBP inertia and CG position coming from filter estimation resulted in

$$\hat{\mathbf{I}} = \begin{bmatrix} 3.436 & 0.356 & 0.210 \\ 0.356 & 12.563 & -0.030 \\ 0.210 & -0.030 & 12.734 \end{bmatrix} \text{ kg m}^2$$
$$\hat{\mathbf{R}}_{CG} = \begin{bmatrix} -7.975 & -9.337 & -8.650 \end{bmatrix}^T 10^{-6} \text{ m} \tag{39}$$

while the standard deviation for these parameters were

$$\boldsymbol{\sigma}_{\mathbf{I}} = \begin{bmatrix} 0.04433 & 0.01016 & 0.01561 \\ 0.01016 & 0.16876 & 0.00516 \\ 0.01561 & 0.00516 & 0.16755 \end{bmatrix} \text{ kg m}^2$$
$$\boldsymbol{\sigma}_{\mathbf{R}CG} = \begin{bmatrix} 1.463 & 0.701 & 1.256 \end{bmatrix}^T 10^{-6} \text{ m} \tag{40}$$

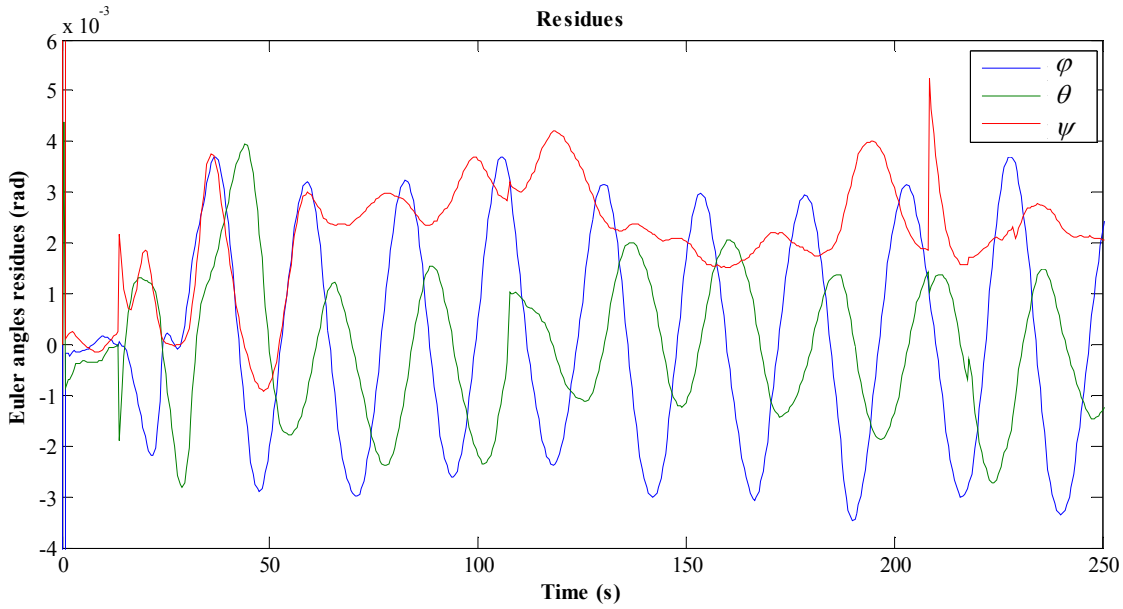

Figure 8. Euler angles residues during the estimation process.

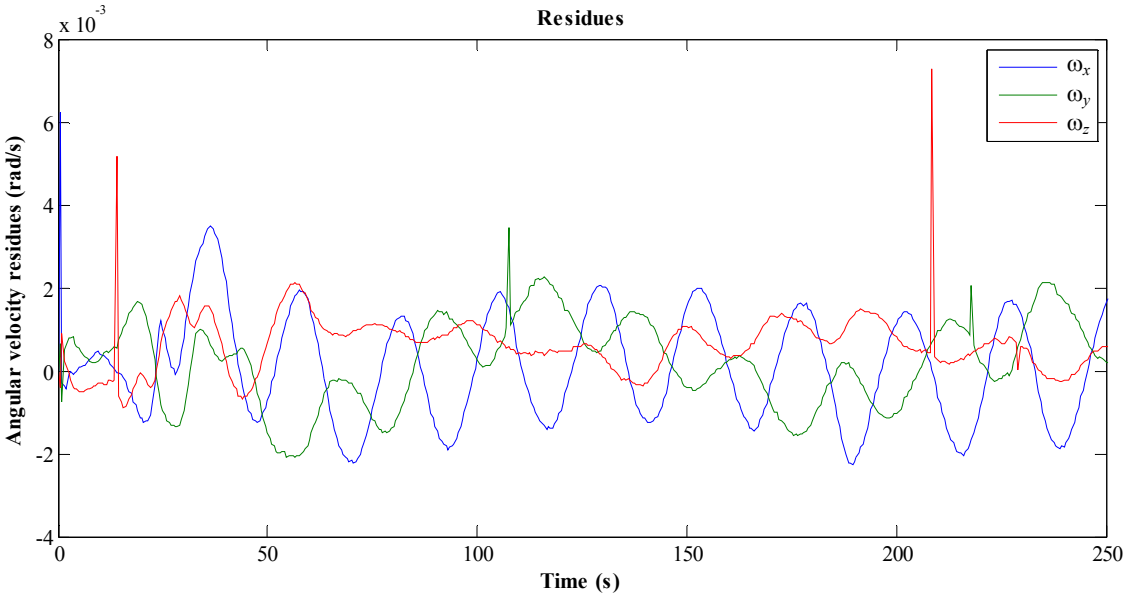

Figure 9. Angular velocity residues during the estimation process.

The values for moments of inertia are slightly larger than the CAD model. This fact was already expected since cables and some pre-balancing masses were used to make a primary balancing in the GBP. Although the CAD computed inertia was a full matrix, the filter was initialized with null values for the products of inertia, because they are small when compared with the moments of inertia. Of course the CAD layout was done taking into account not only

balancing of the GBP but also the alignment between the platform reference axes and the axes of the principal moment of inertia.

CONTROL ALGORITHM USING REACTION WHEELS

Since the GBP shall be used as a development test bed for AOCS subsystems, an attitude controller was implemented and tested. The control employs the reaction wheels as unique actuators, and the gyros and star sensor as attitude sensors. A PD (Proportional-Derivative) controller was chosen and integrated to the PCDH. The integrative portion of the controller is not necessary because the system already has a pole at the origin and thus the error is zero for a step input. The control diagram can be seen in Figure (10). J stands for the moment of inertia at a given axis, and b represents a viscous friction coefficient between the GBP and air, causing a torque proportional to the angular velocity. The constants k_p and k_d are the proportional and derivative gains. As for disturbance torque it was considered in the model just the misalignment between the bearing center and the platform center of gravity. Except for the viscous friction coefficient, all other coefficients were estimated or calculated.

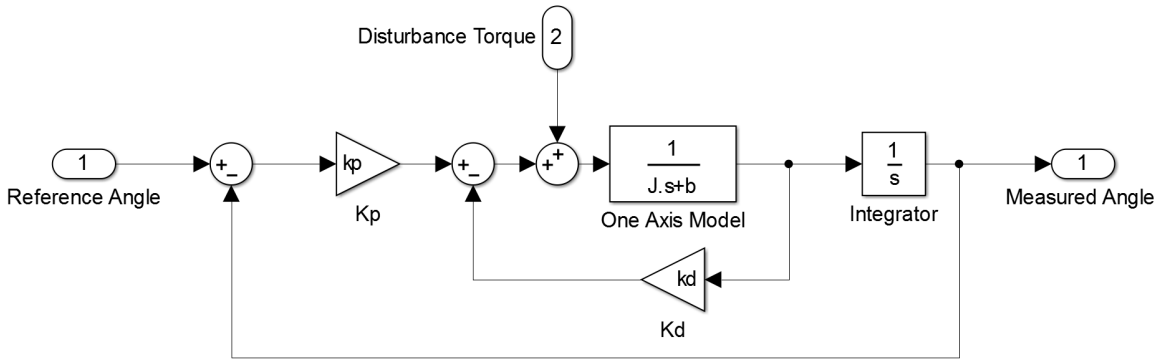

Figure 10. Simple control algorithm for the GBP.

Two simplifying assumptions were made in order to approximate the nonlinear dynamics of rotation to a linear and uncoupled system. The first one was to consider negligible the products of inertia, and so the inertia matrix became diagonal. The second was to admit that the body rotation rate is very small. These two assumptions together greatly reduce the non-linear portion of the system and makes uncoupling between body axes possible. The controller design, then, was done separately for each axis. The gains for the 3-axes controller were computed so as to give a control response with a 10% overshoot and settling time of 100 seconds. The proportional gains are, for x, y and z axes: 0.01573, 0.05751 and 0.05830 Nm/rad, while the derivative gains are 0.27388, 1.00404, and 1.01772 Nms/rad. Moreover, the adopted viscous coefficient for all axes is 0.001 Nms/rad.

The GBP was commanded to perform a 180 degrees rotation about z-axis. Figures (11), (12) and (13) show the response of the platform to the controller action. The attitude in Euler angles is presented in Figure (11), while Figures (12) and (13) present the angular velocity (gyro measurements) and commanded reaction wheel torques, respectively. Unfortunately, due to bad weather conditions during several nights at the time of this writing, the star sensor could not be used in this experiment. The attitude controller had to rely only on the gyro measurements, and this explains the reason why the initial attitude is zero. It is remarkable that the torque saturates quickly, as soon as the control begins to maneuver the GBP, as can be seen in Figure (13).

Probably due to the saturation of the reaction wheel torque the overshoot was slightly reduced when compared to the design values. In fact, the measured overshoot in *z*-axis was only 7.5%. The measured settling time of 101.6 s, on the other hand, was close to the design one. However it was expected a bigger time, due to the torque saturation.

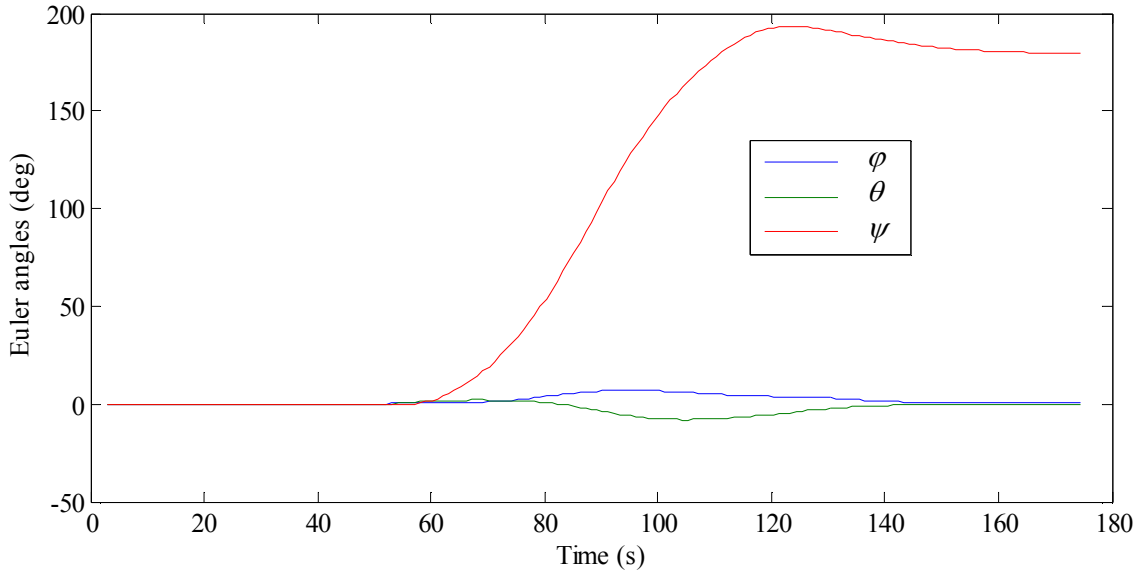

Figure 11. GBP attitude of a 180° *z*-axis maneuver.

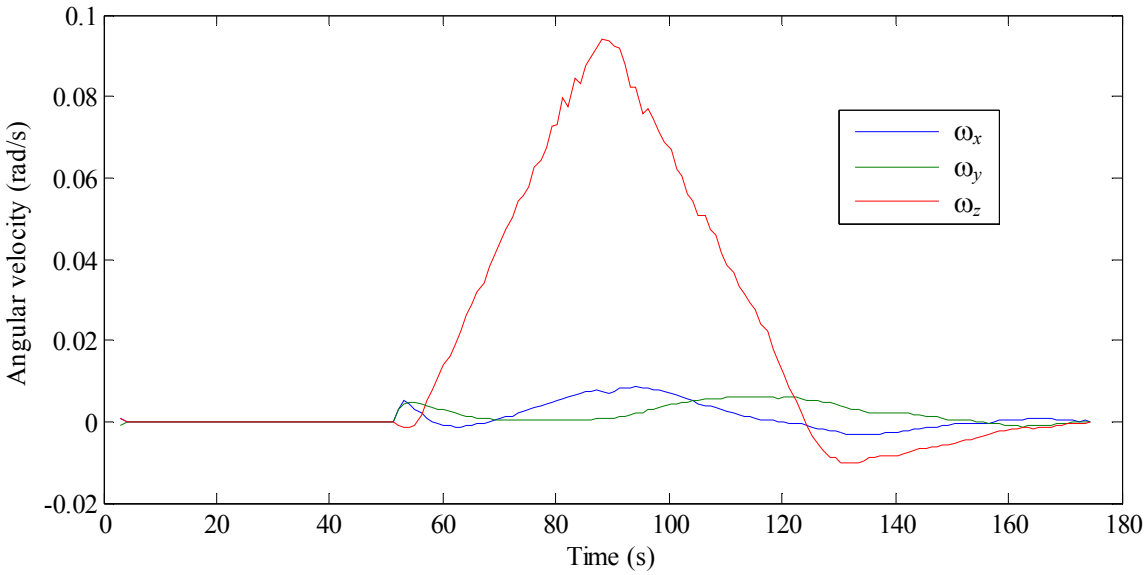

Figure 12. GBP angular velocity during maneuver.

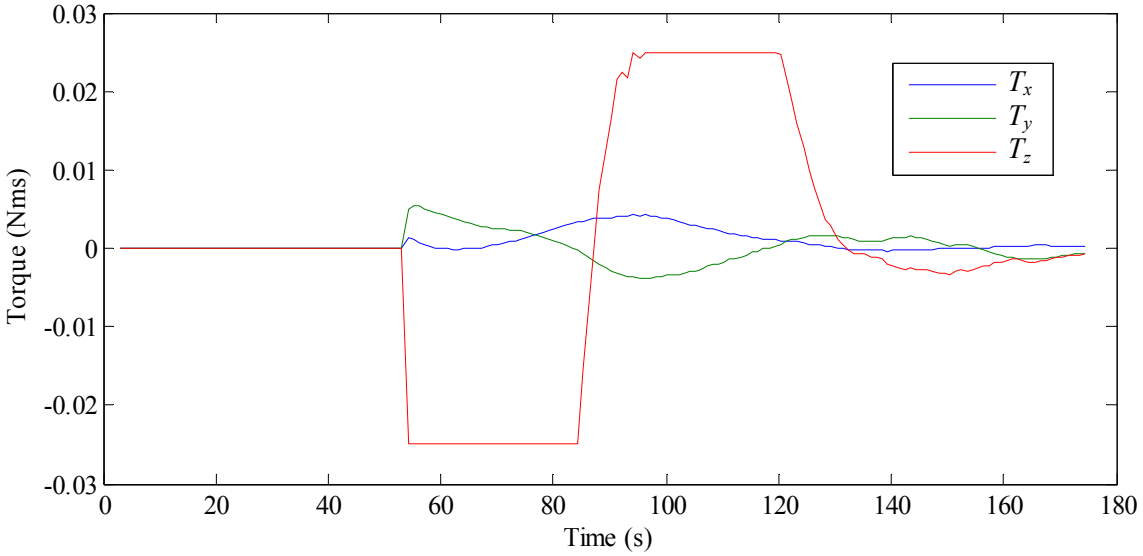

Figure 13. Applied reaction wheel torque. Saturation limits the torque to 0.025 Nm.

CONCLUSION

This work presented the efforts being carried out in Brazil to achieve an in house technology for a 3-axis stabilized and digitally controlled satellite attitude. These efforts were directed to a Gas Bearing Platform equipped with attitude sensors and actuators, which allow reasonable simulation of the space environment. The sensors are composed of a gyroscope triad, a star sensor, a 3-axis magnetometer and a GPS receiver. As well 3 reaction wheels and a set of 3 magnetic torquers generate the control action.

In order to calibrate the gyros, a linear model was settled and the calibration parameters were obtained by least squares fitting from several data collected by an accurate servo-controlled 3-axis turntable. The estimated gyro parameters were the scale factor and alignment matrix, and bias vector. They were obtained with many different calibration sequences, with six distinct configurations in order to excite all axes.

The scale factors and bias obtained here will be obviously slightly different if the experiment was repeated with another calibration sequence. This can be explained by the noise model of the sensors, which are a composition of quantization noise, random walk and bias instability, besides the already modeled ones. They could be reached by processing the Allan Variance for the individual gyros, but it is outside the scope of this paper.

As expected, after calibration the gyroscope triad still presents a drift of few degrees per hour, which is the best nonmilitary precision that can be achieved in the industry for inertial measurement units. Gyro sensors with drift in the order of degrees per day or better are usually employed in space applications.

Although the calibration process was done with the gyros turning only around the vertical axis, the model parameters obtained by calibration can always improve the angular position measurement at the end of a short time integration process. So a periodic attitude determination with the star sensor or magnetometer plus sun sensors (or accelerometer, if a GBP is being

considered) shall be necessary. The calibrated gyroscope triad was then used in experiments involving attitude determination, estimation of mass properties (inertia and CG position), and attitude control.

An extended Kalman filter was employed to estimate the GBP inertia and CG. The inertia matrix had a good agreement with the CAD model, which provided an initial guess for inertia in the filtering process. The estimated offset of the CG resulted in few micrometers, as expected after a manual but quite precise balancing of the GBP.

Together with pointing and control requirements, the estimated GBP moments of inertia were used to calculate the gains of a proportional-derivative attitude controller. The analysis of the GBP response under the effect of the designed controller gains contributed to validate the estimated mass properties.

The PD attitude control was successfully applied to an onboard algorithm for a 3-axis attitude control of the GBP. The controller's response was satisfactory and the small differences between the control design and control response can be explained by model simplification and the non-linear platform dynamics. Despite being a very simple experiment, the platform, allied to the sensors and actuators, proved to be a reliable and truly reproduces the space environment allowing simulating not only all the attitude control system but also the real attitude dynamics. It can be used to test complex control algorithms with real sensors and actuators, as well as to validate and to qualify satellite attitude control systems. This platform can also be used to test algorithms for reaction wheel de-saturation, a fairly common problem in 3-axis stabilized satellites.

Finally, it is worth to mention that this work is the first initiative of a 3-axis satellite attitude controller performed in Brazil, and surely shall be an invaluable test bed for attitude control development to help future Brazilian space missions.

ACKNOWLEDGMENTS

Authors acknowledge support and funding by project FUNDEP-FINEP-SIA-11382*3 and INPE.

REFERENCES

[1] Schwartz, J. L., Peck, M. A., Hall, C. D. “Historical Survey of Air-Bearing Spacecraft Simulators”, Journal of Guidance, Control, and Dynamics, Vol. 26, No 4, 2003, pp. 513-522.

[2] Rizos, I., Arbes, J., and Raoult, J., “A Spherical Air Bearing Supported Test Facility for Performance Testing of Satellite Attitude Control Systems,” Proceedings of the 4th International Federation of Automatic Control Symposium on Automatic Control in Space, Austria, 1971, pp. 341–348.

[3] Snider, R. E. “Attitude Control of a Satellite Simulator Using Reaction Wheels and a PID Controller”. Air Force Institute of Technlology, Wright-Patterson Air Force Base, Ohio, 2010. AFIT/GAE/ENY/10-M24.

[4] Agrawal, B., Rasmussen, R., “Air Bearing Based Satellite Attitude Dynamics Simulator for Control Software Research and Development”, Proceedings of the SPIE Conference on Technologies for Synthetic Environments, Vol. 6, Washington, USA, 2001, pp. 204–214.

[5] Kim, B., Velenis, E., Kriengsiri, P., Tsiotras, P., “A Spacecraft Simulator for Research and Education”, Proceedings of the AIAA/AAS Astrodynamics Specialists Conference, No. AAS 01-367, Quebec, Canada, 2001, pp. 897–914.

[6] Schwartz, Jana L., Hall, Christopher D., “Comparison of System Identification Techniques for a Spherical Air-Bearing Spacecraft Simulator”, Proceedings of the AAS/AIAA Astrodynamics Conference, No. AAS 03-611, Montana, USA, 2003.

[7] Gelb, A. “Applied Optimal Estimation”. Ed. MIT Press, MA, USA, 384p, 1974.

[8] Lefferts, E. J., Markley, F. L., Shuster, M. D. “Kalman filtering for spacecraft attitude estimation”. Vol. 5, N. 5, 1962, pp. 417-429.

[9] Hugues, P. C., “Spacecraft Attitude Dynamics”, Ed. Dover Publications, New York, USA, 592p, 1986.

[10] Wertz, J. R., “Spacecraft Attitude Determination and Control”, Ed. Kluwer Academic Publishers, Dordrecht, The Netherlands, 876p, 1978.

[11] Aguirre, L. A. “Introduction to Systems Identification” (in Portuguese), 3rd. Edition, Ed. UFMG, Minas Gerais, Brazil, 730p, 2007.

[12] Maybeck, P. S. “Stochastic Models, Estimation, and Control”, Ed. Academic Press, Vol. 1, New York, USA, 423p.,1979.

[13] Schedlinski, C.; Link, M. “A Survey of Current Inertia Parameter Identification Methods”. Mechanical Systems and Signal Processing, Vol. 15, N. 1, 2001. pp. 189-211.